CC17 group B *Streptococcus* exploits integrins for neonatal meningitis development

Romain Deshayes de Cambronne,[1] Agnès Fouet,[1] Amandine Picart,[1] Anne-Sophie Bourrel,[1,2] Cyril Anjou,[1] Guillaume Bouvier,[3] Cristina Candeias,[1] Abdelouhab Bouaboud,[1] Lionel Costa,[1] Anne-Cécile Boulay,[4] Martine Cohen-Salmon,[4] Isabelle Plu,[5] Caroline Rambaud,[6] Eva Faurobert,[7] Corinne Albigès-Rizo,[7] Asmaa Tazi,[1,2,8] Claire Poyart,[1,2,8] and Julie Guignot[1]

[1]Université de Paris, Institut Cochin, INSERM, U1016, CNRS, UMR8104, Paris, France. [2]Hôpitaux Universitaires Paris Centre, Cochin, Assistance Publique Hôpitaux de Paris, France. [3]Structural Bioinformatics Unit, Department of Structural Biology and Chemistry, Institut Pasteur, CNRS UMR3528, C3BI, Paris, France. [4]Center for Interdisciplinary Research in Biology (CIRB), Collège de France, CNRS UMR7241, INSERM U1050, PSL Research University, Paris, France. [5]Sorbonne Université/Département de Neuropathologie Raymond Escourolle — Hôpital Pitié-Salpêtrière — Assistance Publique-Hôpitaux de Paris, France. [6]Université de Versailles Saint Quentin en Yvelines (Université Paris-Saclay)/Service d'anatomie-pathologique et médecine légale, Hôpital Raymond Poincaré, Garches, France. [7]INSERM U1209, CNRS UMR 5309, Institute for Advanced Biosciences, France/Université Grenoble Alpes, La Tronche, France. [8]Centre National de Référence des Streptocoques, France.

Group B *Streptococcus* (GBS) is the major cause of human neonatal infections. A single clone, designated CC17-GBS, accounts for more than 80% of meningitis cases, the most severe form of the infection. However, the events allowing blood-borne GBS to penetrate the brain remain largely elusive. In this study, we identified the host transmembrane receptors α5β1 and αvβ3 integrins as the ligands of Srr2, a major CC17-GBS–specific adhesin. Two motifs located in the binding region of Srr2 were responsible for the interaction between CC17-GBS and these integrins. We demonstrated in a blood-brain-barrier cellular model that both integrins contributed to the adhesion and internalization of CC17-GBS. Strikingly, both integrins were overexpressed during the postnatal period in the brain vessels of the blood-brain barrier and blood-cerebrospinal fluid barrier and contributed to juvenile susceptibility to CC17 meningitis. Finally, blocking these integrins decreased the ability of CC17-GBS to cross into the CNS of juvenile mice in an in vivo model of meningitis. Our study demonstrated that CC17-GBS exploits integrins in order to cross the brain vessels, leading to meningitis. Importantly, it provides host molecular insights into neonate's susceptibility to CC17-GBS meningitis, thereby opening new perspectives for therapeutic and prevention strategies of GBS-elicited meningitis.

Introduction

In the early 1950s, because of the massive utilization of tetracyclines, *Streptococcus agalactiae* (group B *Streptococcus*, GBS) emerged worldwide as the most significant pathogen causing severe neonatal invasive infections (1). This commensal bacterium, which is found in the intestine and the genital tract of 11% to 22% of healthy humans (2), is responsible for 2 syndromes in neonates, early-onset disease (EOD), which occurs within the first 48 hours after birth in 90% of cases, and late-onset disease (LOD), which occurs between 7 and 89 days of life (3). EOD results from mother-to-child vertical transmission of the bacterium through the inhalation of GBS-contaminated amniotic fluid or vaginal secretions during delivery. EOD often manifests by bloodstream infections that are complicated by meningitis in 15% to 30% of the cases (4). The onset of LOD remains largely unknown, although recent studies argue for the coexistence of intrapartum and postnatal transmission routes and for a gastrointestinal portal of entry (5–7). Meningitis is common during LOD, in up to 50% of cases, mainly due to one particular GBS clone almost exclusively of capsular serotype III and belonging to clonal complex 17 (CC 17). Overall, as reported by worldwide epidemiological studies, the so-called hypervirulent CC17-GBS is responsible for 80% to 95% of cases of neonatal GBS–elicited meningitis, for EOD and LOD combined, highlighting a strong meningeal tropism (4, 8–11).

The critical step for meningitis development is the transmigration of blood-borne GBS into the CNS. The brain is normally protected by physiological barriers that separate the blood from the brain parenchyma or the cerebrospinal fluid. Brain microvascular endothelial cells and choroid plexus epithelial cells that compose the blood-brain barrier (BBB) and the blood-cerebrospinal fluid barrier (BCSFB), respectively, are characterized by the presence of tight junctions that are crucial for the maintenance of the barrier function. To penetrate those barriers, blood-borne bacteria can either use a transcellular mechanism that requires pathogen internalization and/or a paracellular mechanism that requires tight-junction disruption. Alternatively, bacteria can use phagocytes as Trojan horses (12). GBS has been described to be internalized in cerebral endothelial cells, but also to inhibit tight-junction protein expression, suggesting that GBS could use transcellular and/or paracellular mechanisms to penetrate the brain (13, 14).

CC17 strains have been shown to display higher adherence properties to brain endothelial cells compared with non-CC17 strains (15). Two CC17-GBS–specific surface adhesins, Srr2 and HvgA, account for the increased binding of CC17-GBS to brain

Conflict of interest: The authors have declared that no conflict of interest exists.

Submitted: January 27, 2020; **Accepted:** January 13, 2021; **Published:** March 1, 2021.
Reference information: *J Clin Invest*. 2021;131(5):e136737.
https://doi.org/10.1172/JCI136737.

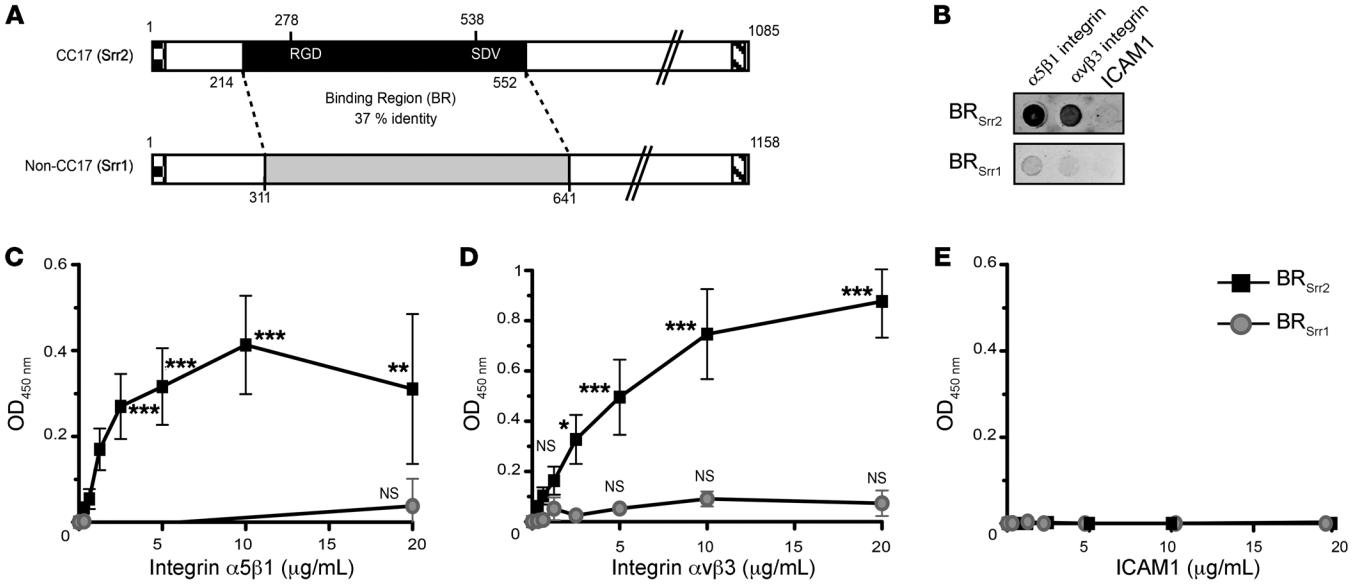

Figure 1. BR_{Srr2} recognizes α5β1 and αvβ3 integrins in a direct manner. (**A**) Schematic representation of Srr2 and Srr1 proteins with signal sequence (checkered), serine-rich regions (white), LP × TG cell wall anchoring motif (hatched), and the binding regions of Srr2 (black) or Srr1 (gray) delineated by dashed lines. Numbers in black indicate the position of amino acid residues, and letters in white indicate the predicted motifs of interaction with integrins. (**B**) Dot blotting was performed to determine the interaction between immobilized human α5β1 and αvβ3 integrins or ICAM1 and BR_{Srr2} or BR_{Srr1}. Purified BR_{Srr2} and BR_{Srr1} proteins are shown in Supplemental Figure 1A. (**C**–**E**) Interaction of BR_{Srr2} (black squares) or BR_{Srr1} (gray circles) with human α5β1 integrin (**C**), αvβ3 integrin (**D**), or ICAM1 (**E**) were assessed by ELISA. Results were normalized to negative control (BSA). Statistical analysis: data shown are mean ± SEM of at least 3 independent experiments. Two-way ANOVA with Bonferroni's multiple-comparison posttest was performed. NS, nonsignificant; $*P < 0.05$; $**P < 0.01$; $***P < 0.001$.

endothelial cells compared with non-CC17 strains and contribute to BBB crossing in an in vivo model of meningitis (15, 16). However, how these proteins contribute to brain barrier crossing at the molecular level is currently unknown.

Here, we demonstrated that Srr2 directly and specifically bound to integrins α5β1 and αvβ3, thereby contributing to the adhesion and invasion of brain endothelial cells and to the crossing of the brain barrier, leading to meningitis development. Most importantly, we showed that these receptors were overexpressed during the postnatal period in brain vessels. This likely accounts for the CC17-GBS increased invasiveness of the CNS in neonates.

Results

The binding region of the Srr2-CC17–specific adhesin interacts with α5β1 and αvβ3 integrins. In contrast to HvgA, for which no molecular ligand has been identified, Srr2 contains a fibrinogen-binding site within the binding region (BR_{Srr2}) involved in CC17-GBS adhesion to a variety of host cells (16–19). An Srr2-homologous protein, designated Srr1, which also possesses a fibrinogen-binding site in its binding region (BR_{Srr1}), is expressed by non-CC17 GBS isolates. Although Srr2 and Srr1 have a similar structure, they display only 37% amino acid sequence identity in their binding regions (Figure 1A). Looking in BR_{Srr2} for binding motifs that could account for the hyperadhesion phenotype properties of CC17-GBS to the host cell, we identified by sequence analysis Arg-Gly-Asp (RGD) and Ser-Asp-Val (SDV) motifs, which are absent from BR_{Srr1} (Figure 1A). These 2 motifs are known to allow integrin recognition (20, 21). Integrins are transmembrane heterodimeric receptors composed of 1 α and 1 β subunit that combine to form up to 24 integrins. The SDV motif has been recently identified to be specific to αvβ3, whereas the RGD motif is recognized by a number of integrins (22, 23). We therefore focused our study on α5β1 and αvβ3 integrins known to recognize RGD or SDV motifs and to be expressed by brain endothelial cells because CC17 strains are highly correlated with meningitis (24, 25).

We therefore compared the interaction of BR_{Srr2} and BR_{Srr1} with α5β1 and αvβ3 integrins. We first measured by immunoblotting the direct binding of BR_{Srr2} and BR_{Srr1} to immobilized recombinant soluble human integrins α5β1 and αvβ3. Intense signals were obtained with BR_{Srr2} where α5β1 and αvβ3 integrins were spotted but not where ICAM1, another transmembrane protein, was spotted, indicating that BR_{Srr2} bound to recombinant human α5β1 and αvβ3 integrins (Figure 1B). In contrast, weak signals were observed when BR_{Srr1} was assayed in the same conditions with α5β1 and αvβ3 integrins (Figure 1B).

The interaction between BR_{Srr2} and human α5β1 and αvβ3 integrins was further confirmed by ELISA assays showing that recombinant human α5β1 and αvβ3 integrins bound to immobilized BR_{Srr2} in a saturable and dose-dependent manner, whereas they failed to bind to BR_{Srr1} (Figure 1C and 1D). As a control, ICAM1 bound neither to BR_{Srr2} nor to BR_{Srr1} (Figure 1E). Moreover, no interaction was observed between the α5β1 and αvβ3 integrins and HvgA, the other CC17-GBS–specific adhesin (data not shown).

Integrin structure and ligand binding affinity are strongly affected by divalent cation concentrations (26). This property was confirmed for BR_{Srr2}-integrin interaction by ELISA assays in the presence of $CaCl_2$ or $MnCl_2$. Addition of Ca^{2+} or Mn^{2+} totally abolished α5β1 integrin binding to BR_{Srr2}, while Ca^{2+} strongly enhanced αvβ3 integrin binding to BR_{Srr2} (Supplemental Figure 2, A and B; supplemental material available online with this article; https://doi.org/10.1172/JCI136737DS1). Last, the interaction between BR_{Srr1}

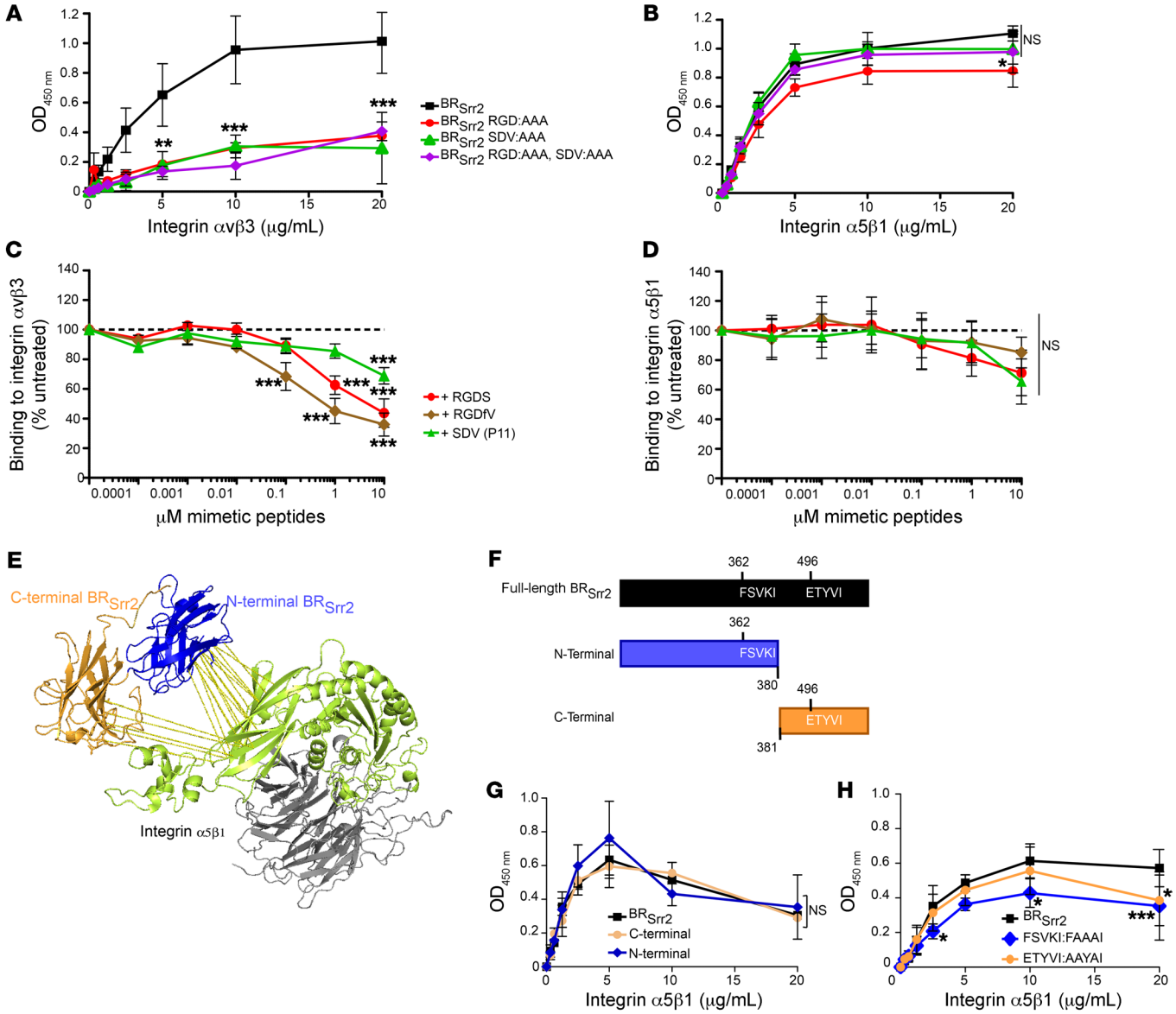

Figure 2. Identification of BR_{Srr2} residues involved in the direct interaction with αvβ3 and α5β1 integrins. (**A** and **B**) Interaction of BR_{Srr2} or its mutated forms with integrins αvβ3 (**A**) or α5β1 (**B**) assessed by ELISA. Mutated forms of BR_{Srr2} proteins are shown in Supplemental Figure 1, B and C. (**C** and **D**) Interaction of BR_{Srr2} with integrins αvβ3 (**C**) or α5β1 (**D**) in the presence of increasing concentration of mimetic peptides assessed by ELISA. Results are expressed as percentage of untreated condition. (**E**) Graphic representation of predicted contacts between BR_{Srr2} and α5β1 integrin identified by RaptorX (Supplemental Figure 4). RaptorX mapped on the α5 (gray) and β1 (green) integrin subunits predicted 2 contact zones located in the N-terminal (blue) and C-terminal (gold) domains of BR_{Srr2}. Only the most reliable contacts (contact probability > 0.7) are depicted as yellow lines in the scheme. (**F**) Schematic representation of BR_{Srr2} or its truncated forms. Numbers in black indicate the position of amino acid residues in Srr2, and letters in white indicate the predicted motifs of interaction with the integrin α5β1. (**G**) ELISA assays with integrin α5β1 were performed using equimolar amounts of coated BR_{Srr2} or of its truncated forms. (**H**) Interaction of BR_{Srr2} or its mutated forms with the integrin α5β1 was assessed by ELISA. Mutated forms of BR_{Srr2} proteins are shown in Supplemental Figure 1, D and E. ELISA results were normalized to the negative control (BSA). Statistical analysis: data shown are mean ± SEM of at least 3 independent experiments. Two-way ANOVA with Bonferroni's multiple-comparison posttest performed. NS, nonsignificant; $*P < 0.05$; $**P < 0.01$; $***P < 0.001$.

and BR_{Srr2} with non-RGD–recognizing integrins expressed by brain endothelial cells (α6β1, α4β1, and α3β1) and non-RGD–recognizing integrins described as directly binding to GBS (α1β1) were analyzed (24, 27). Interestingly, both BR_{Srr1} and BR_{Srr2} interacted with α6β1, α4β1, and α3β1 integrins; however, this was not a general feature of all the integrins because α1β1 failed to bind both BR_{Srr1} and BR_{Srr2} (Supplemental Figure 3). Altogether, our data showed that α5β1 and αvβ3 integrins were directly and specifically recognized by BR_{Srr2}.

αvβ3-BR_{Srr2} interaction depends on the RGD and SDV motifs. In order to test the role of the RGD and SDV motifs present on BR_{Srr2} in their interaction with integrins, mutated forms of BR_{Srr2} were produced in which the RGD and/or SDV motifs were replaced by 3 alanines (Supplemental Figure 1B and C). The interaction between BR_{Srr2} mutated forms with integrins αvβ3 or α5β1 was assessed by ELISA. RGD and/or SDV substitutions strongly affected αvβ3 integrin binding (Figure 2A) but not α5β1 integrin binding (Figure 2B).

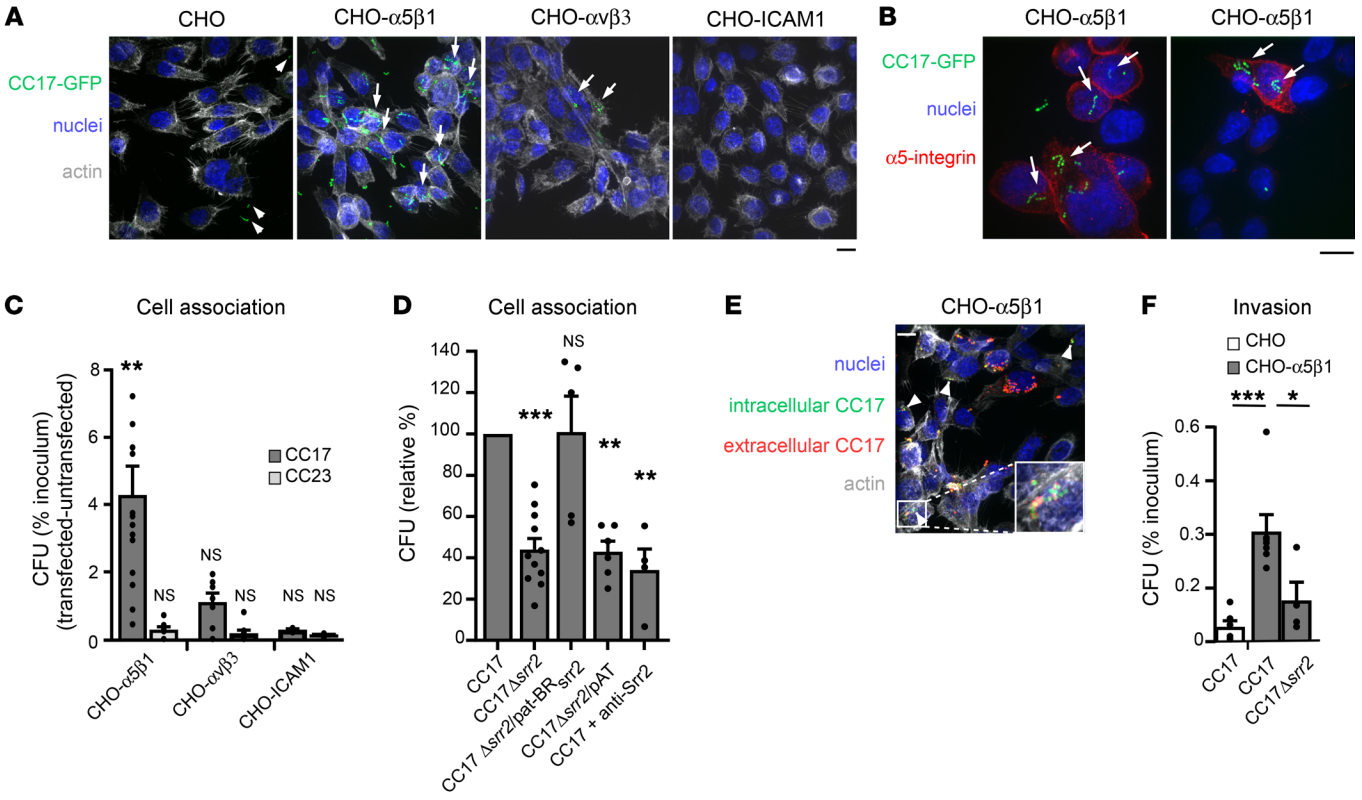

Figure 3. α5β1 promotes adhesion and invasion of CC17-GBS in a simplified model of CHO cells. (**A** and **B**) CHO, CHO-α5β1, CHO-αvβ3, and CHO-ICAM1 were infected with GBS strains for 1 hour, and then analyzed by (**A**, **B**, and **E**) immunofluorescence or (**C**, **D**, and **F**) CFU counts. (**A**) Representative micrographs of untransfected or transfected CHO cells infected with CC17-GFP (green). Nuclei were labeled with DAPI (blue) and actin with phalloidin (gray). Scale bar: 10 μm. (**B**) Representative micrographs of transfected CHO-α5β1 infected with CC17-GFP strain (green) and immunostained with anti–α5 integrin antibody (red). Two independent fields from the same experiment are shown. Scale bar: 10 μm. (**C**) Adhesion of a CC17 or a non-CC17 (CC23) strain on transfected or untransfected CHO cells was quantified. Results are expressed as the percentage of adhesion obtained on transfected cells minus that obtained on untransfected cells. (**D**) Adhesion level of WT CC17 and derived strains on CHO-α5β1 normalized to WT CC17 adhesion. Anti-Srr2 antibody was diluted 1:500. (**E**) CC17-GFP strain (green) was used to infect CHO-α5β1. Differential staining was used to distinguish extracellular from intracellular bacteria. GBS outside of host cells have green (GFP) and red fluorescence (anti-GBS) and appear yellow/red, whereas bacteria inside host cells have green fluorescence only. Nuclei were labeled with DAPI (blue) and actin was stained using phalloidin (gray). Scale bar: 10 μm. Boxed area corresponds to magnification of inset. (**F**) Invasion of CC17 strain or Δ*srr2*-derived strain on untransfected CHO or CHO-α5β1 was quantified by CFU counts. All experiments were performed at least 3 times with each condition. Statistical analysis: Data shown are mean ± SEM of at least 3 independent experiments realized in triplicate. One-way ANOVA with Tukey's (**C** and **F**) or Dunn's (**D**) multiple-comparison test was performed. NS, nonsignificant; $^*P < 0.05$; $^{**}P < 0.01$; $^{***}P < 0.001$.

No additive inhibition was observed when both motifs (RGD and SDV) were mutated (Figure 2A).

The contribution of these motifs to integrin binding was further supported by competitive ELISA assays using synthetic peptides containing an RGD sequence (RGDS and RGDfV peptides) or an SDV sequence (P11 peptide) widely used to inhibit integrin recognition (20, 21). RGD and SDV peptides significantly inhibited αvβ3-BR_{Srr2} interaction in a dose-dependent manner, whereas they had no significant effect on α5β1-BR_{Srr2} interaction (Figure 2, C and D). Altogether, these results demonstrated that the interaction of BR_{Srr2} with integrin αvβ3 required both RGD and SDV motifs, whereas the interaction with integrin α5β1 was independent from these motifs.

BR_{Srr2} interaction with integrin α5β1 involves 2 other motifs. To identify BR_{Srr2} residues involved in α5β1 integrin recognition, we used the RaptorX web server that enables, by combining coevolution and deep learning, the prediction of residue-residue interactions (28). Using this approach, 2 putative motifs of interaction between BR_{Srr2} and α5β1 were identified (Supplemental Figure 4A and Figure 2E). The first was an FSVKI motif located in the N-terminal subdomain of BR_{Srr2} at position 362 and the second was an ETYVI motif located in the C-terminal subdomain of BR_{Srr2} at position 496 (Figure 2, E and F). These 2 motifs are absent from the BR_{Srr1} sequence. To address the role of these 2 motifs in the interaction with integrin α5β1, we first addressed the binding capacities of BR_{Srr2} subdomains containing these motifs. The N-terminal and C-terminal subdomains of BR_{Srr2} containing either motif were produced, and an equimolar amount of full-length BR_{Srr2}, N-terminal, and C-terminal domains was used to perform ELISA binding assays. The α5β1 integrin displayed a similar capacity to bind to all 3 forms of BR_{Srr2} (Figure 2G), indicating the presence of at least one binding motif on each BR_{Srr2} subdomain.

We next generated mutated forms of BR_{Srr2} in which the FSVKI or the ETYVI sequences were replaced by FAAAI and AAYAI, respectively (Supplemental Figure 1, D and E), and the interaction with integrin α51 was assessed by ELISA. Although the mutation of the ETYVI

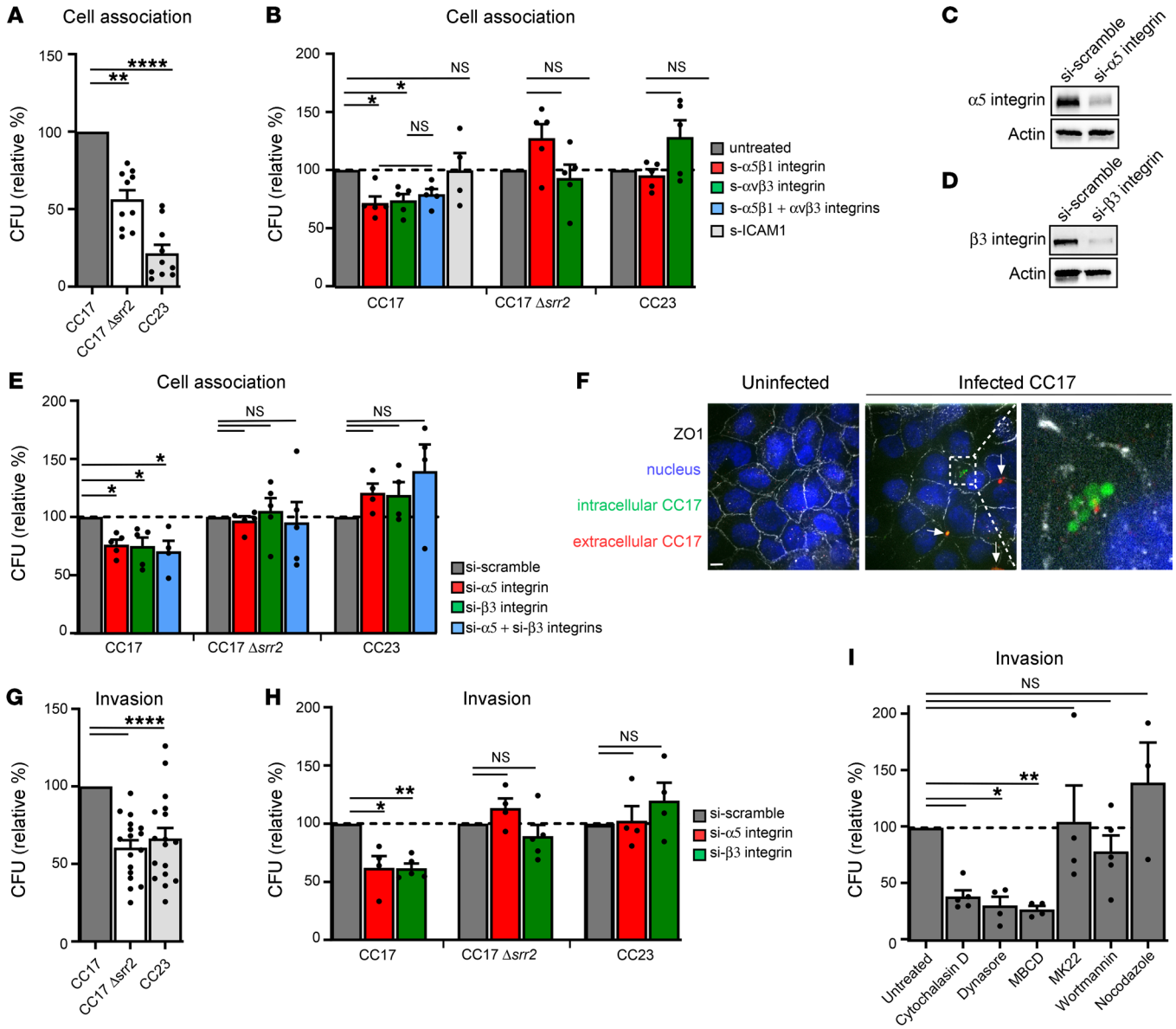

Figure 4. α5β1 and αvβ3 integrins promote Srr2-dependent CC17-GBS attachment and invasion of cerebral endothelial cells. (**A** and **B**) Adhesion of GBS strains onto hCMEC/D3 was assessed by CFU counts (**A**) at MOI 10 and (**B**) at MOI 1 in the absence or presence of 10 μg/mL of recombinant human soluble α5β1 (s-α5β1 integrin) or αvβ3 (s-αvβ3 integrin), or a mix of both integrins (s-α5β1 + s-αvβ3 integrins), or ICAM1 (s-ICAM1). For each strain, results were normalized to those obtained in the control experiment (untreated). (**C** and **D**) Depletion of relevant integrin subunit in siRNA knockdown of (**C**) α5 integrin and (**D**) β3 integrin in hCMEC/D3 analyzed by Western blot. (**E**) Adhesion of GBS strains onto cerebral endothelial cells, control (si-scramble), α5 integrin–depleted (si-α5 integrin), β3 integrin–depleted (si-β3 integrin), and α5 integrin– and β3 integrin–depleted (si-α5 + si-β3 integrins) quantified by CFU after 1 hour infection. For each strain, results were normalized to those obtained in the control experiment (si-scramble). (**F**) CC17-GFP strain (green) was used to infect cerebral endothelial cells. Differential staining was used to differentiate intracellular (green) from extracellular (green + red) bacteria as in Figure 3E. Nuclei: DAPI (blue) and ZO1 (gray). Scale bar: 5 μm. (**G**) Invasion of GBS strains in hCMEC/D3 was quantified by CFU counts. (**H**) Invasion of GBS strains in hCMEC/D3. For each strain, results were normalized to those obtained in the control experiment (si-scramble). (**H**) Invasion of CC17 strain in hCMEC/D3 was realized in the presence of host cell signaling inhibitors and normalized to untreated condition. Statistical analysis: Experiments were performed at least 3 times with each condition in triplicate and expressed as mean ± SEM. One-way ANOVA with Dunn's multiple-comparison test was performed. NS, nonsignificant; $^{*}P < 0.05$; $^{**}P < 0.01$; $^{****}P < 0.0001$.

motif affected the interaction with α5β1 integrin only at the highest concentration, the mutation of the FSVKI motif significantly reduced the binding to α5β1 integrin at most concentrations (Figure 2H).

Altogether, we identified the FSVKI motif of BR_{Srr2} as required for α5β1 integrin recognition. In addition, we demonstrated that BR_{Srr2} contains at least one other integrin α5β1 recognition motif, which is located in its C-terminal region but remains to be identified. Interestingly, when integrin-binding motifs were highlighted on BR_{Srr2}, we noticed that both αvβ3 binding motifs (RGD and SDV) were localized on the same side of BR_{Srr2}, whereas the α5β1 binding motif, FSVKI, was located on the opposite side (Supplemental Figure 4B).

Human α5β1 integrin acts as a receptor for Srr2-expressing GBS in a simplified model of Chinese hamster ovary cells. To determine whether α5β1 and αvβ3 integrins are viable candidate receptors for adhesion and/or invasion of CC17-GBS, the binding of a CC17-GBS strain to a simplified model where cells ectopically express human α5β1 or αvβ3 integrins was assessed. We infected the Chinese hamster ovary (CHO) control cell line, which does not express endogenous β3 or α5 integrin subunits and is therefore deficient in the expression of α5β1 and αvβ3 integrins (29), or CHO cells stably transfected with plasmids encoding human α5β1 (CHO-α5β1), human αvβ3 (CHO-αvβ3), or human ICAM1 as a control (30–32).

Numerous CC17-GBS bacteria were observed adhering to CHO-α5β1 cells (Figure 3A arrows) as compared with nontransfected CHO or CHO-ICAM1 cells that were nonpermissive for CC17 adhesion where most streptococci were found unbound to cells (Figure 3 A, arrowheads). Immunostaining with anti-α5 antibody showed that CC17-GBS bacteria were almost exclusively associated with cells expressing integrin α5β1, whereas few bacteria were associated with cells that had lost its expression (Figure 3B). In addition, few CC17-GBS bacteria adhered to CHO-αvβ3 (Figure 3A). However, only the adhesion to α5β1-expressing cells was statistically significant (Figure 3C). We next analyzed the specificity of CC17-GBS interaction with α5β1 integrin by testing adhesion of a non-CC17 GBS strain (CC23) expressing the Srr1 surface protein to CHO transfected cells. The CC23-GBS strain did not show proficient adhesion to any CHO cell lines tested (Figure 3C). Altogether, these results indicate that integrin α5β1 is an effective and specific host receptor for CC17-GBS.

To demonstrate that the binding to α5β1 integrin by CC17-GBS was dependent on Srr2, we tested the adhesion of CC17 Δ*srr2*–derived strains. The adhesion of the Δ*srr2* mutant strain to CHO-α5β1 revealed a clear defect when compared with that of the isogenic WT strain. Complementation of the Δ*srr2* mutant with a plasmid expressing the BR_{Srr2} domain was sufficient to restore adhesion to the WT level. In agreement with this result, adhesion of CC17-GBS to CHO-α5β1 was inhibited by anti-Srr2 antibody. Altogether, these data demonstrated that Srr2 was responsible for CC17-GBS adhesion to α5β1 integrin (Figure 3D).

Finally, using differential staining to distinguish extracellular from intracellular streptococci, we were able to detect internalized CC17-GFP bacteria in CHO-α5β1 cells (Figure 3E). Comparing invasion rates obtained with CHO-α5β1 and with untransfected cells, CFU counting indicated that α5β1 integrin also promoted CC17-GBS internalization in an Srr2-dependent manner (Figure 3F). In conclusion, our data demonstrated that Srr2 expression allowed α5β1 integrin recognition, promoting CC17-GBS adhesion and invasion in a simplified cellular model.

α5β1 and αvβ3 integrins promote CC17-GBS's binding to and invasion of cerebral endothelial cells. Blood-borne CC17-GBS must interact with the luminal face of cerebral endothelial cells to access the CNS. Because integrins are known to be expressed on the luminal and abluminal faces of endothelial cells (33–36), we addressed the role of integrins in a more physiologically relevant model of cerebral endothelial cells. We previously showed that CC17-GBS displayed a hyperadhesion phenotype on cerebral endothelial cells compared with non-CC17 GBS strains (15). The CC17-specific adhesins HvgA and Srr2 contribute to the adhesion properties of CC17-GBS (15, 17). Therefore, we proposed to address the role of Srr2-integrin interaction in CC17-GBS adhesion to cells of the BBB. Using the human cerebral microvascular endothelial cell line hCMEC/D3, we first confirmed that CC17-GBS adheres in an Srr2-dependent manner more than the non-CC17 strain (CC23) (Figure 4A). Because the expression of bacteria recognizing cellular receptors may change upon infection, we analyzed integrin expression. Expression of α5β1 and αvβ3 was not modified by infection with CC17-GBS for up to 3 hours at the transcriptional level (Supplemental Figure 5, A and C) or at the protein level (Supplemental Figure 5, B and D). To investigate whether α5β1 and αvβ3 integrins could contribute to CC17 hyperadhesion to brain endothelial cells, we performed competition experiments with soluble integrins. When CC17-GBS bacteria were preincubated with soluble human α5β1 or αvβ3 integrins, CC17 adhesion to hCMEC/D3 was significantly reduced compared with that of the untreated control (Figure 4B). No additive effect was observed when α5β1 and αvβ3 integrins were mixed. As a control, preincubation with soluble ICAM1 did not alter CC17-GBS adhesion. Neither α5β1, nor αvβ3 integrins, nor ICAM1 soluble protein affected the adhesion of the Δ*srr2* mutant or that of non–CC17-GBS (Figure 4B), indicating that the adhesion of CC17-GBS to hCMEC/D3 cells depended on Srr2-α5β1 and Srr2-αvβ3 interactions.

To confirm the role of α5β1 and αvβ3 integrins in CC17-GBS adhesion to hCMEC/D3, we silenced integrin expression by transfecting endothelial cells with specific siRNAs. Because integrins are composed of 1 α chain and 1 β chain that combine to form heterodimers, we targeted the α5 chain to silence α5β1 and the β3 chain to silence αvβ3, a strategy that minimizes side effects on other integrins. The effect of siRNA-mediated silencing of α5 or β3 chains was efficient as evidenced by Western blot analysis (Figure 4, C and D). When α5 or β3 expression was silenced, CC17-GBS adhesion was significantly reduced compared with scramble control-transfected cells. No additive effect was observed when both α5 and β3 were simultaneously silenced. In contrast, adhesion of the Δ*srr2* mutant strain or the non–CC17-GBS strain was not affected by α5 or β3 integrin silencing (Figure 4E).

Finally, we investigated the contribution of Srr2-integrin interactions in cellular barrier crossing. Indeed, bacterial adhesion to brain endothelial cells is a prerequisite for the crossing of the BBB by either a paracellular or transcellular mechanism. When brain microvascular endothelial cells were infected with the CC17 strain for 1 hour, no obvious disruption of the ZO1 tight-junction protein was observed (Figure 4F). Furthermore, staining allowing the differentiation of extracellular from intracellular bacteria revealed the presence of intracellular bacteria, suggesting a transcellular passage (Figure 4F). We therefore compared the invasion by a CC17-GBS strain to that of the Δ*srr2* and non–CC17-GBS strains (Figure 4G). Invasion of the WT CC17 strain was higher than that of the other strains, demonstrating the existence of an Srr2-dependent invasion (Figure 4G). We thus assayed the consequences of siRNA silencing of α5 or β3 expression on CC17-GBS internalization. The invasion level of CC17-GBS was significantly reduced in α5 and β3 silenced cells (Figure 4H). In contrast, internalizations of the Δ*srr2* mutant and the non–CC17-GBS strains were unmodified (Figure 4H). To analyze the CC17-GBS internalization

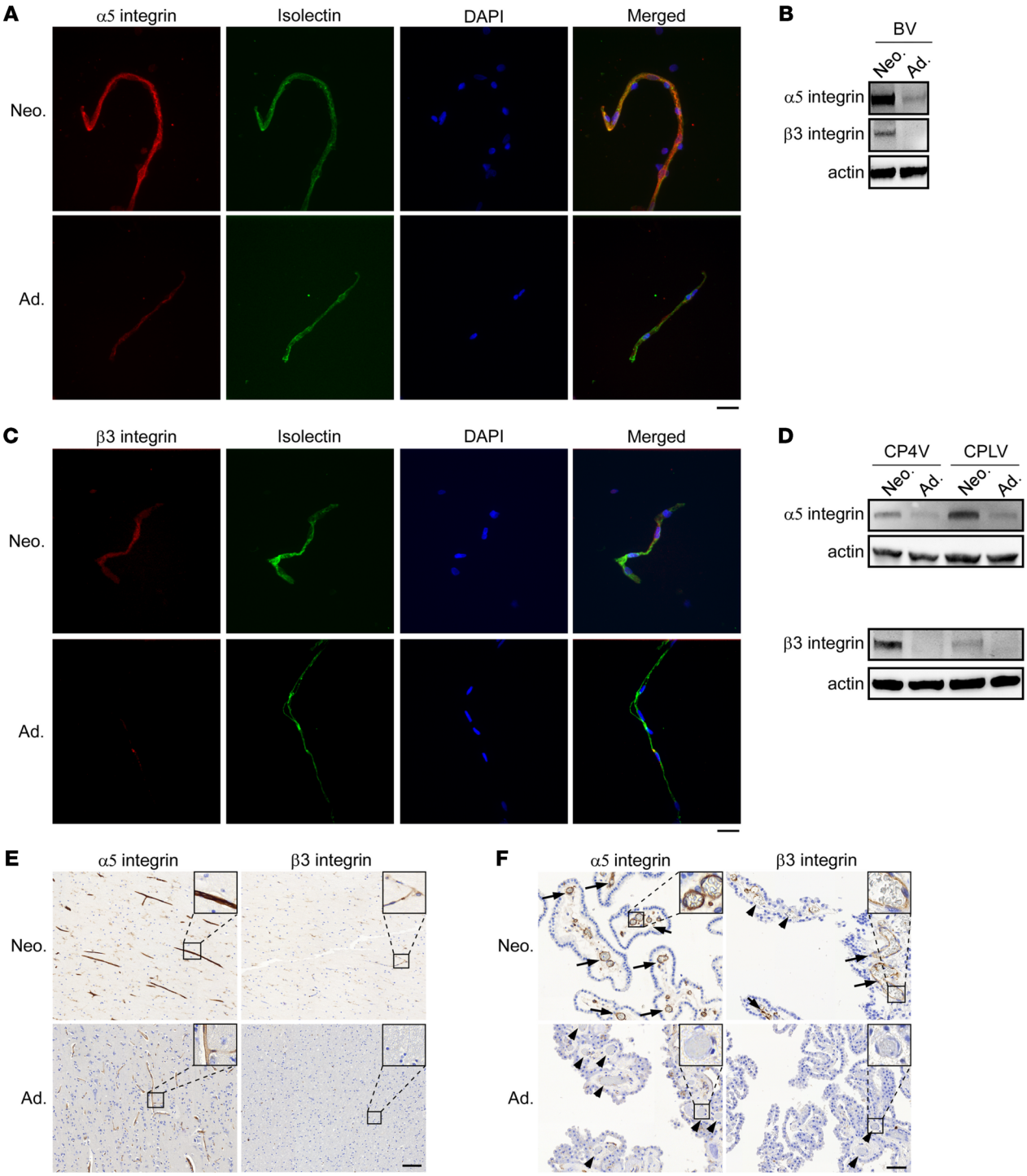

Figure 5. α5β1 and αvβ3 integrins are overexpressed during the postnatal period. Expression of α5β1 or αvβ3 integrins in neonates (Neo.) or adults (Ad.) were analyzed by (**A** and **C**) immunofluorescence (n = 2), (**B** and **D**) Western blot (n = 3), or (**E** and **F**) immunohistochemistry (n = 2). (**A** and **B**) Purified rat brain vessels (BV) were labeled with specific antibodies against (**A**) α5 integrin to visualize α5β1 expression or (**B**) β3 integrin to visualize αvβ3 expression. BV were counterstained using FITC–isolectin B4 and nuclei were labeled with DAPI. Scale bar: 20 μm. Similar contrast adjustment was applied between neonate and adult images. (**C** and **D**) 100 μg of rat (**C**) BV or (**D**) choroid plexus from fourth ventricle (CP4V) or lateral ventricles (CPLV) were analyzed by Western blot. Actin was used as loading control. (**E** and **F**) Sections of human brain tissue were analyzed by immunohistochemistry using antibodies against α5 or β3 integrins to visualize α5β1 or αvβ3, respectively, and then counterstained with hematoxylin. Representative micrographs of cortex allowing visualization of (**E**) BV (scale bar: 100 μm) or (**F**) choroid plexuses (scale bar: 50 μm). Arrows indicate BV from choroid vessels displaying positive staining; arrowheads indicate BV displaying negative staining. Boxed areas correspond to magnification of insets.

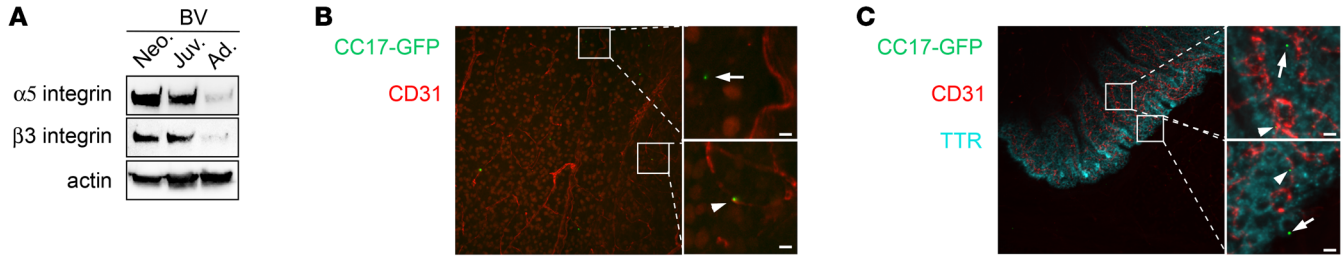

Figure 6. Initial brain penetration of CC17-GBS occurs via blood vessels from the cortex and the choroid plexuses. Expression of α5β1 or αvβ3 integrins on purified brain vessels (BV) from neonatal (Neo.), juvenile (Juv.), or adult (Ad.) BALB/c mice analyzed by Western blot (n = 2). (**A**) Juvenile mice were infected for 4 hours with CC17-GFP strain (green) (n = 2). Cerebral blood vessels were stained with CD31 (red) and choroid plexus with anti-TTR (cyan). Cortex (**B**) and choroid plexuses from the lateral ventricles (**C**) were examined. CC17-GFP bacteria were found associated with blood vessels (arrowheads) and at distance from blood vessels (arrows). Scale bar: 5 μm.

process in hCMEC/D3 and the putative involvement of signal transduction molecules involved in integrin signaling, we performed invasion assays in the presence of various inhibitors. The actin-depolymerizing agent (cytochalasin D), the cholesterol-depleting agent (methyl-β-cyclodextrin), and the dynamin-2 inhibitor (dynasore) inhibited CC17-GBS invasion. In contrast, the microtubule-depolymerizing agent (nocodazole), the PI3 kinase inhibitor (wortmannin), and the Akt inhibitor (MK22) had no effect (Figure 4I). Altogether, these results indicate that the Srr2 adhesin expressed by CC17-GBS used α5β1 and αvβ3 integrins to promote the adhesion of CC17 strains on cerebral endothelial cells, leading to their internalization by a mechanism involving actin, dynamin-2, and lipid rafts.

α5β1 and αvβ3 integrins are overexpressed during the postnatal period. CC17-GBS is overrepresented among GBS neonatal meningitis, accounting for more than 80% of the cases (4, 9, 11). In contrast, epidemiological data show that GBS is an uncommon cause of meningitis in adults and CC17 is only found in 21% of the cases (37, 38). Meningeal pathogens can enter the brain via the BBB and/or the BCSFB located in the choroid plexuses of the ventricular area (12). We therefore hypothesized that neonatal susceptibility to CC17-GBS meningitis might be correlated with the expression of α5β1 and αvβ3 integrins at the BBB/BCSFB level. To test this hypothesis, cerebral blood vessels from neonatal and adult rats were purified and the expression of α5β1 and αvβ3 was assessed by immunofluorescence staining and Western blot analysis. A striking, intense α5 integrin staining was observed on brain vessels from pups, whereas adult brain vessels displayed a much less intense staining (Figure 5A). Overexpression of α5 integrin in neonatal brain vessels was confirmed by Western blot analysis (Figure 5B). Although no β3 expression was detected on adult brain vessels, either by immunofluorescence or by Western blot, a faint but easily detectable β3 expression was observed in brain vessels from rat pups (Figure 5, B and C). These results indicate that α5β1 and αvβ3 integrins are overexpressed in rat brain vessels during the neonatal period.

Choroid plexuses are composed of blood vessels that are different from those of the BBB, and of stroma and choroid epithelial cells that form the BCSFB (39). Therefore, choroid plexus tissues from the fourth ventricle (CP4V) or the lateral ventricles (CPLV) were collected and analyzed for α5 and β3 expression. We found that α5 integrin was overexpressed in rat pups compared with adults, and β3 integrin expression could only be detected in the choroid plexuses of rat pups (Figure 5D).

Importantly, similar results were obtained for human brain samples by immunohistochemistry analyses of the brain of a newborn (9 days old) and an adult (52 years old), for whom the causes of death were unrelated to meningitis. In the cortex, α5 integrin staining mainly revealed cerebral blood vessels in the neonate and adult. However, the staining intensity of the cerebral blood vessels was strikingly more intense in the neonatal cortex compared with the adult. In the neonate, β3 expression was very faint and observed in slightly bigger blood vessels than capillaries, whereas it was totally absent in the adult cortex (Figure 5E).

When brain sections from the ventricular area were specifically analyzed for α5 expression, a massive staining of all choroid plexus blood vessels was observed in the human neonatal specimen (Figure 5F, arrows). In contrast to and except for a few infiltrating cells, α5 expression was not detected in the adult specimen (Figure 5F, arrowheads). Similar to what was observed in the cortex, β3 expression was restricted to the biggest blood vessels in the choroid plexuses (Figure 5F, arrows) and absent from smaller blood vessels (Figure 5F, arrowheads), whereas it was totally absent in the adult choroid plexuses (Figure 5F). Importantly, neither α5 nor β3 integrins were detected in choroid plexus epithelial cells of either the neonate or the adult (Figure 5F). Altogether, these data indicate that α5β1 and αvβ3 integrins are overexpressed in human blood vessels of the BBB and the BCSFB during the neonatal period.

Initial brain penetration of CC17-GBS occurs at the BBB and BCSFB. CC17-GBS bacteria have been associated with brain vessels of the BBB and the choroid plexus of the BCSFB in a fatal case of neonatal LOD (15). However, the initial portal of entry of GBS in the brain remains unknown. To determine the initial entry site of CC17-GBS, we used an in vivo murine bacteremia-derived meningitis model (6, 16). To carry out the experiments on a more amenable model than neonatal mice, we tested the presence of α5β1 and αvβ3 integrins in the brain vessels of juvenile mice. These integrins were also still expressed at a high level in juvenile mice compared with adult mice (Figure 6A). Four hours after i.v. injection of juvenile mice with the CC17-GFP strain, bacteria were found outside the blood vessels in the cortex and the choroid plexuses (Figure 6, B and C), indicating successful transmigration of CC17-GBS to the CNS at both the BBB and the BCSFB.

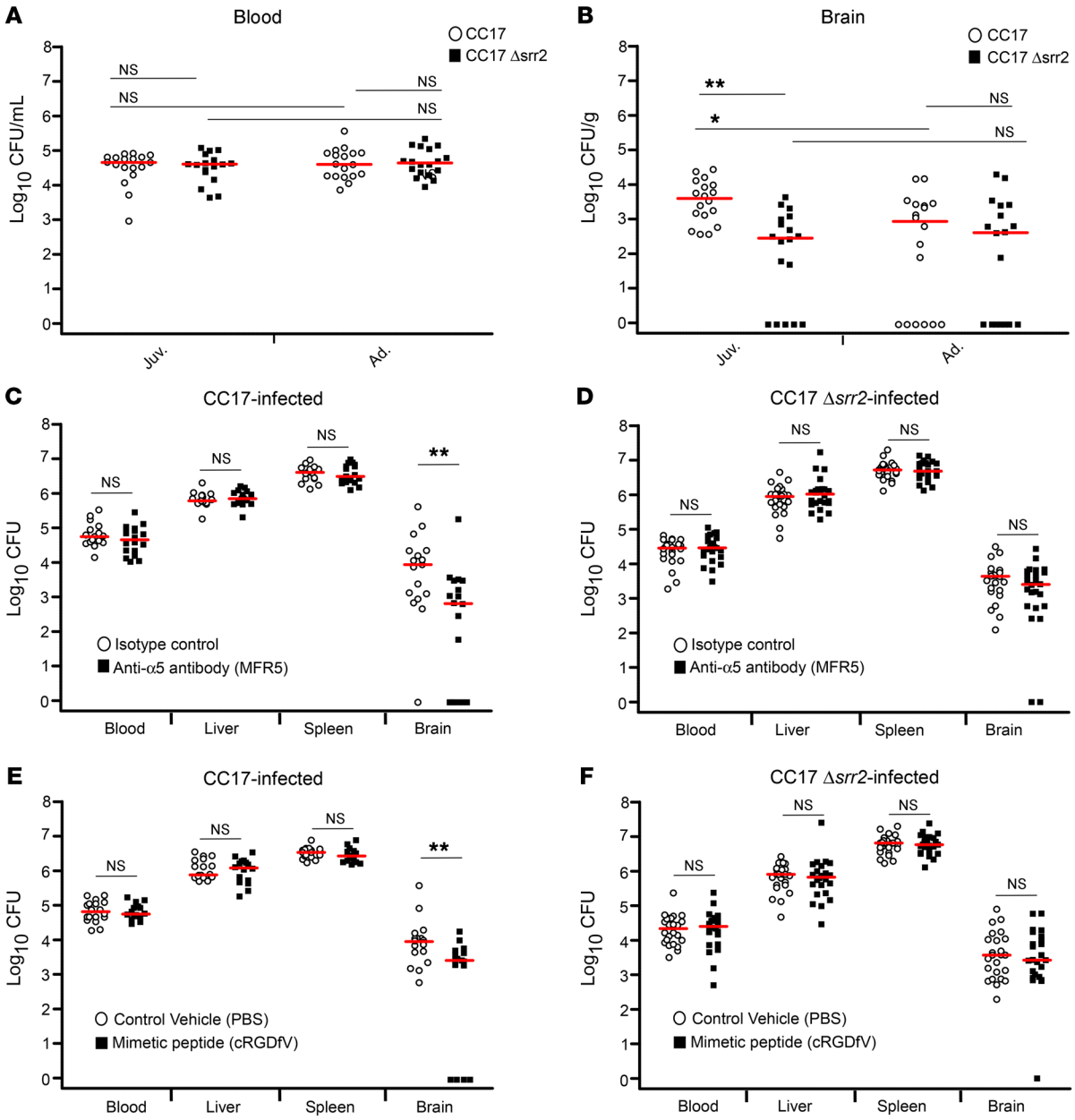

Figure 7. α5β1 and αvβ3 integrins contribute to juvenile-specific CC17-GBS–elicited meningitis in vivo. Juvenile or adult BALB/c mice were infected by i.v. injection with WT CC17 (white circles) or Δ*srr2* mutant (black squares) for 4 hours. Mice were euthanized and bacterial loads in blood (CFU/mL) (**A**) and brain (CFU/g) (**B**) were quantified. Each symbol represents the numeration from 1 organ from 1 mouse. Red horizontal lines indicate medians. Statistical analysis: 2-way ANOVA with Bonferroni's posttest was performed. NS, nonsignificant; $^{*}P < 0.05$; $^{**}P < 0.01$. Juvenile BALB/c mice were pretreated by (**C** and **D**) i.v. injection of 10 μg of anti-α5 antibody to block α5β1 integrin or 10 μg of isotype control, or (**E** and **F**) 5 mg/kg of RGDfV mimetic peptide to block αvβ3 or control vehicle (PBS). One hour after pretreatment, mice were infected by i.v. injection with 2×10^7 CFU of WT CC17 (**C** and **E**) or Δ*srr2* mutant (**D** and **F**) for 4 hours. Mice were euthanized, and bacterial loads in blood (CFU/mL), spleen, liver, and brain (CFU/g) were quantified. Each symbol represents the numeration from 1 organ from 1 mouse. White circles: control mice; black squares: treated mice. Red horizontal lines indicate medians. Statistical analysis: Mann-Whitney *U* test; NS, nonsignificant; $^{*}P < 0.05$; $^{**}P < 0.01$.

In vivo, α5β1 and αvβ3 integrins are involved in juvenile susceptibility to CC17-GBS meningitis. Next, we studied the relevance of the interaction between Srr2 adhesin and α5β1 and αvβ3 integrins in vivo. We first controlled the ability of BR_{Srr2} to recognize murine α5β1 and αvβ3 integrins, validating the use of the murine model (Supplemental Figure 6). We compared the susceptibility to CC17-GBS meningitis of juvenile mice to that of adult mice. In order to specifically address transmigration capacity to the CNS, we adapted the experiment to have the same bacteremia in juvenile and adult mice. We found that infection with 2×10^7 CFU in juvenile mice and 1.5×10^8 CFU in adult mice gave similar bacteremia at 4 hours after infection (Figure 7A). Four hours after i.v. infection with WT bacteria, significantly fewer bacteria were recovered from the brain of adult mice than of juvenile mice, demonstrating that juvenile mice were more susceptible to CC17 meningitis than adult mice (Figure 7B). We thus assayed the requirement for the Srr2

adhesin in meningitis development in juvenile and adult mice and found that significantly fewer Δ*srr2* than WT bacteria were recovered from the brain of juvenile mice (Figure 7B). In contrast, similar bacterial counts of the WT and the Δ*srr2* mutant were recovered from adult brains (Figure 7B). Furthermore, and whereas such was not the case with juvenile mice, 33% of adult mice infected with the WT strain had a bacteria-free brain, as in Δ*srr2*-infected juvenile and adult mice (38% and 27% respectively). These results demonstrated that Srr2 adhesin contributed to the early event of CC17-GBS transmigration to the CNS in juvenile mice and did not contribute to the milder CNS transmigration in adult mice.

We therefore addressed the role of the integrins α5β1 and αvβ3 in the Srr2-dependent susceptibility of juvenile mice. To establish the contribution of integrin α5β1, and since α5-integrin-KO mice are embryonically lethal (40), we developed a model based on the use of blocking antibody, a strategy successfully used for other meningeal pathogens (41). Anti–α5 integrin neutralizing antibody or isotype control antibody–treated mice were i.v. infected with CC17-GBS. The resulting bacteremia and total CFU counts 4 hours after infection in the spleen and liver were similar, but significantly reduced in the brain as compared with the control condition (Figure 7C). In contrast, anti–α5 integrin neutralizing antibody did not affect the capacity of the Δ*srr2* mutant to reach the brain in that similar bacterial counts were recovered from the brain of anti-α5–pretreated mice compared with the control condition (Figure 7D).

Similarly, because β3-integrin-KO mice suffer from vascular leakage (42), a blocking strategy was also used to investigate the αvβ3 integrin role in the early event of CC17-GBS transmigration to the CNS. Integrin αvβ3 was blocked using the mimetic peptide RGDfV, which was highly efficient at inhibiting the BR_{Srr2}-αvβ3 interaction in vitro (Figure 2C). RGDfV mimetic peptide or control vehicle-treated mice were infected with CC17-GBS. Administration of RGDfV mimetic peptide had no effect on bacteremia, spleen, and liver CFU counts 4 hours after infection, yet decreased CC17-GBS penetration of the brain compared with the control vehicle (Figure 7E) but not the Δ*srr2* mutant (Figure 7F). Together, our data demonstrated that Srr2 interaction with α5β1 and αvβ3 integrins contributed to the susceptibility of juvenile mice to CC17-GBS meningitis and that pretreatments targeting these integrins reduced brain invasion.

Discussion

Neonatal bacterial meningitis is a devastating life-threatening infection of the CNS. Despite antenatal screening of pregnant women associated with intrapartum antibiotic prophylaxis for GBS-positive mothers in most high-income countries, GBS remains the leading cause of neonatal meningitis. Meningitis cases due to GBS are accompanied by neurological complications, including seizure, hydrocephalus, subdural empyema, or cerebrovascular diseases, and lead to 10% mortality and 25% permanent sequelae in surviving babies (43–45). Deciphering the mechanisms that drive the initial step of brain penetration by identifying the bacterial ligands and their cognate host cell receptors is of major clinical importance.

In our study, we demonstrated that the Srr2 adhesin, specifically and exclusively expressed by the hypervirulent CC17-GBS clone, mediated bacterial binding to brain endothelial cells by interacting with the cellular host receptors, integrins α5β1 and αvβ3. This interaction was essential for CC17-GBS to adhere to and invade brain endothelial cells and contributed to meningitis development in vivo. Using a simplified cellular model, we demonstrated that α5β1 integrin was sufficient to promote CC17-GBS adhesion and internalization. In contrast, although recognized by Srr2 and being involved in adhesion and internalization into hCMEC/D3 and in meningitis development in vivo, αvβ3 integrin was not sufficient to trigger CC17-GBS adhesion and internalization in a cellular simplified model. This indicates that α5β1 integrin is stricto sensu a receptor for CC17-GBS, while αvβ3 integrin likely acts as a coreceptor as described for other pathogens (46). We also noticed that blocking the Srr2-integrin interaction of the WT CC17 strain, by competition with soluble integrins or by siRNA, did not reduce binding or invasion levels as much as deleting *srr2*. This could be explained either by the fact that blocking was not 100% efficient or by the fact that Srr2 could recognize receptors other than α5β1 and αvβ3. Srr2 adhesin harbors 2 distinct binding motifs, RGD and SDV, which interact with the αvβ3 integrin. Although numerous bacterial adhesins have been described to harbor an RGD motif, Srr2 is, to our knowledge, the first example of a bacterial adhesin harboring an SDV motif, which is a newly described integrin binding motif (22). We have also shown, via an in silico approach confirmed by in vitro experiments, that Srr2 harbors 2 others motifs required for direct binding to the α5β1 integrin, one in the N-terminal and one in the C-terminal subdomain of BR_{Srr2}. We have identified FSVKI as an important motif present on the N-terminal domain of BR_{Srr2} for α5β1 integrin recognition. The pathophysiological relevance for the presence of 2 binding sites for each integrin is intriguing, but has been described for other bacterial adhesins, e.g., from group A *Streptococcus* that possesses several integrin-binding sites on the same adhesin (47, 48). This probably reveals the importance of integrin recognition by those pathogens in the pathophysiology of the infection.

Our study highlights the role of integrins in the internalization process of CC17-GBS into endothelial cells. Although we did not investigate further the internalization mechanism, we found that inhibitors of PI3K or Akt, which are molecules involved in integrin signaling, are not required for CC17-GBS internalization; rather, CC17-GBS internalization seems to be dependent on actin cytoskeleton, dynamin-2, and lipid rafts, as already described for other pathogens interacting with integrins (49).

How recognition of integrins by Srr2 adhesin enables bacterial entry into the brain is an important question that remains to be determined. On peripheral endothelial cells, bacterial adhesin-integrin interactions have been shown to promote bacterial vascular transmigration (50, 51). However, our current models of cerebral endothelial cells are not appropriate to investigate the CC17-GBS transmigration mechanism. This could occur by a transcellular and/or paracellular mechanism. Indeed, a transcellular crossing of the BBB has been described by Nizet et al. (14). But integrins are also known to be interconnected to cell junctions, therefore being able to affect the vascular permeability in peripheral and brain endothelial cell monolayers, which would lead to a paracellular transmigration for GBS (52–56). The latter has not been described upon GBS infection, yet some tight-junction modifications upon

GBS infection have been observed at time points later than 1 hour (13, 57). Although speculative, direct Srr2-integrin interaction could therefore, in addition to CC17-GBS internalization in endothelial cells, lead to vascular permeability alteration favoring GBS paracellular transmigration at later time points. This hypothesis is reinforced by the fact that CC17-GBS strains strongly bind to fibrinogen in an Srr2-dependent manner (16, 17). On endothelial cells, α5β1 and αvβ3 integrins are host receptors for fibrinogen. Fibrinogen fixation on its cellular receptors also leads to vascular permeability (58). Fibrinogen could therefore potentiate vascular permeability by acting as a bridging molecule between CC17-GBS and integrins, an indirect mechanism for integrin recognition largely employed by pathogens (59).

It has been shown that at the BBB, GBS exploits α2β1 integrin in an indirect manner through collagen recognition (60). However, collagen recognition by GBS is not a conserved phenotype among GBS strains (61). This suggests that α2β1 integrin recognition is likely not a generalized mechanism to GBS strains. GBS also exploits α1β1 integrin in the vaginal tract (27, 62). However, α1β1 integrin is not expressed by brain endothelial cells (25), and we showed that neither Srr2 nor Srr1 bound α1β1 integrin (Supplemental Figure 3).

Previous studies highlighted the presence of specific CC17 surface proteins and their role in CC17 neurotropism (15–17, 63). By identifying α5β1 and αvβ3 as specific receptors for Srr2, we provide insights for understanding the neurotropism displayed by CC17 strains compared with other GBS clones. The vast majority of GBS-elicited meningitis occurs during the first 3 months of life (64), and the overwhelming majority of cases are due to the CC17 clone (4, 9, 11). GBS can also cause meningitis or other invasive diseases in adults, particularly among the elderly, those with underlying diseases, or upon consumption of a raw fish meal. However, in adults, the CC17 clone is underrepresented, with most of the infections due to serotype V strains or strains belonging to the ST283 sequence type, the recently identified clone linked to raw fish consumption (38, 65). The reasons that CC17 is overrepresented in newborns compared with adults are largely unknown. We have recently shown that perinatal hormones specifically favor CC17 pathogenesis by promoting the maturation of intestinal M cells responsible for intestinal translocation (6). This present work reveals that α5β1/αvβ3 integrins are overexpressed in neonatal blood vessels of the BBB and BCSFB. The overexpression of α5β1/αvβ3 integrins detected during the neonatal period could be due to the developmental switch of integrin expression occurring during the postnatal period (66). This finding is of major clinical importance because the overexpression observed during the postnatal period corresponds to the peak of CC17-elicited meningitis. Finally, no expression of the α5β1/αvβ3 integrins was detected in choroid plexus epithelial cells. Yet, CC17 bacteria have been closely associated with choroid plexus epithelial cells on brain slices of a fatal case of LOD (15), indicating that CC17 must recognize receptors other than these 2 integrins to cross choroid plexus epithelial cells.

The identification of specific host receptors favoring CC17-GBS brain penetration could represent useful targets for prevention and therapy of GBS meningitis. Indeed, our results showed that pretreatments targeting these integrins can reduce brain invasion. Receptor blockade using antibodies or antagonists in adjunct treatment with antibiotics have high therapeutic potential. Several anti-integrin mAbs or integrin antagonists have been already developed and are currently used in various clinical or preclinical trials (67). The development of novel therapeutic strategies targeting the CC17-GBS is urgent, especially because LOD cases, for which the hypervirulent CC17-GBS is preponderant, have been continuously increasing in the last 20 years (10).

Methods

Bacterial strains, plasmids, primers, and antibodies. Bacterial strains, plasmids, primers, and antibodies used in this study are listed in Supplemental Tables 1, 2, 3, and 4, respectively. *S. agalactiae* strains were cultured in Todd Hewitt (TH) in standing, filled flasks of broth or agar (Difco Laboratories) at 37°C. *Escherichia coli* was cultivated in Luria-Bertani (LB) medium. Antibiotics were used at the following concentrations: for *E. coli*, 100 μg/mL ampicillin; for *S. agalactiae*, 100 μg/mL spectinomycin.

Reagents. Recombinant human ICAM1 and human or mouse integrins (tested by the supplier for their ability to interact with known ligands) were from R&D Systems. The mimetic peptide RGDfV was from Sigma-Aldrich; RGDS and P11 were from Tocris. cOmplete Protease Inhibitor Cocktail (Roche Diagnostics) was used following the manufacturer's instructions.

Expression and purification of His-tagged-BR recombinant peptides. Point mutations in putative integrin-binding sites were inserted by site-directed mutagenesis on pET2818-BR_{Srr2} (16) using the QuikChange II XL Site-Directed Mutagenesis Kit (Stratagene). After verification of the constructs by DNA sequencing, the constructed plasmids were introduced into *E. coli* BL21 for protein expression. Recombinant BR_{Srr2} regions were purified after induction with 1 mM IPTG using Dynabeads (Life Technologies) following the manufacturer's instructions.

ELISA. To evaluate integrin or ICAM1 binding to immobilized BR_{Srr2} or BR_{Srr1} regions, ELISA assays were performed as follows: proteins were coated at 5 μg/mL overnight. After extensive wash and saturation with BSA (Probumin, MilliporeSigma), 50 μL of ligand proteins (human integrins, ICAM1, or negative control BSA) were diluted at the specified concentrations in PBS containing 1% BSA (Probumin) and incubated 2 hours at 37°C. Integrin binding was assessed using antibodies listed in Supplemental Table 4. Binding was detected using *o*-phenylenediamine dihydrochloride (OPD) (Sigma-Aldrich) or 3,3′,5,5′-tetramethylbenzidine (TMB) (Thermo Fisher Scientific). Values of the negative control obtained with BSA (Probumin) were subtracted from the signal. The effect of divalent cations on the interaction between BR_{Srr2} and integrins was tested by ELISA with the same protocol as above in the presence of 1 mM Mn^{2+} or 1 mM Ca^{2+}, as specified. Similarly, competition experiments were carried out by incubating 10 μg of integrins with immobilized BR_{Srr2} in the presence of increasing concentrations of mimetic peptides (RGDS, RGDfV, or P11).

Bioinformatic analysis. In silico contact prediction of BR_{Srr2} (PDB code: 4MBR) interaction with α5β1 integrin (PDB code: 4WJK) was performed using the RaptorX Protein Complex Contact Prediction server (http://raptorx.uchicago.edu/ComplexContact/) (28). Graphical representation of predicted contacts between BR_{Srr2} and α5β1 integrin, identified by RaptorX, was generated using the PyMOL Molecular Graphics System, version 2.0 (Schrödinger, LLC).

Cell lines and culture conditions. (hCMEC/D3 cells were cultured as described previously (68). CHO cells stably transfected with human α5β1, αvβ3, or ICAM1, described and validated previously (30–32), were grown in DMEM containing nonessential amino acids and 5% FCS in the presence of appropriate antibiotic selection pressure. All cell lines were routinely tested for mycoplasma contamination (MycoAlert Mycoplasma Detection Kit, Lonza).

siRNA transfection. To silence the expression of α5 or β3 integrin subunits, pools of 4 siRNA duplexes (ON-TARGET plus SMARTpool siRNA from Dharmacon) were used. The silencer select negative control-1 siRNA (Ambion) was used as negative control. hCMEC/D3 cells were transfected with siRNA using the Nucleofactor Kit UVEC (Amaxa Biosystems), and then seeded at 85,000 cells/cm^2 in 24-well plates for 24 hours. Transfected cells were transfected for a second time with 25 nM siRNA using Lipofectamine RNAiMAX Reagent (Invitrogen) according to the manufacturer's instructions and incubated for a further 24 hours. Cells were used 48 hours after the first transfection. Efficiency of knockdown was assessed by Western blot analysis.

Dot blot and Western blot analysis. For the dot blot assay, 1 μg of human α5β1, αvβ3, and ICAM1 were dotted onto PVDF membranes placed in a Minifold dot blot apparatus SRC-96/1 (Schleicher & Schuell). Strips were blocked with PBS containing 5% skim milk for 1 hour. Interaction between immobilized α5β1, αvβ3, and ICAM1 (negative control) and BR_{Srr2} or BR_{Srr1} was realized by incubating strips overnight at 4°C in PBS containing 2% skim milk and 10 μg/mL of BR_{Srr1} or BR_{Srr2}. After incubation, the strips were washed 3 times in PBS/0.05% Tween, and then incubated with anti-Srr2 or anti-Srr1 antibodies in 5% skim milk for 1 hour at room temperature. Antisera raised against Srr1 and Srr2 are highly specific and display similar affinity (16).

For Western blotting, protein concentration was determined using the BCA protein assay kit (Thermo Fisher Scientific). Proteins were resolved by SDS-PAGE, and then transferred to PVDF membranes using the Trans-Blot Turbo transfer pack (Bio-Rad). Membranes were blocked in PBS containing 5% skim milk and incubated for 1 hour with primary antibodies. Anti-actin directly coupled to HRP was used as a loading control for Western blot.

After washing and incubation with HRP-conjugated secondary antibody (Jackson ImmunoResearch Laboratories), signals from dot blot or membranes from Western blot were revealed using the ECL detection system (PerkinElmer) and signals were detected using a chemiluminescence imaging system (Fusion, Vilber-Lourmat).

Association and invasion assays. Bacterial adhesion or invasion assays were performed in cellular culture media without FCS at an MOI of 10 bacteria per cell unless otherwise specified. Briefly, bacteria were grown to the mid-log phase, washed twice with sterile PBS, and then added to cells and centrifuged 5 minutes at 211*g* to synchronize infection. After 1 hour of incubation at 37°C under a 5% CO_2 atmosphere, monolayers were washed 4 times with PBS. Cell association was determined after lysis with sterile H_2O. Appropriate dilutions were made in sterile PBS, plated on TH agar, and CFUs counted. The percentage of association was calculated as follows: (CFU on plate count/CFU in inoculum) × 100. Assays were performed in triplicate and were repeated at least 3 times. When specified, results were expressed as normalized to the control condition.

For the invasion assay, 1-hour–infected cell monolayers were treated for 30 minutes with cellular culture media containing penicillin/streptomycin (Gibco) and gentamicin (200 μg/mL) to kill extracellular bacteria. The monolayers were washed twice with PBS and lysed with sterile H_2O. Appropriate dilutions were plated on TH agar and CFUs counted. The percentage of invasion was calculated as follows: (CFU on plate count/CFU in inoculum) × 100. Assays were performed in triplicate and were repeated at least 3 times. When specified, results were expressed as normalized to the control condition. To decipher host signaling pathways during CC17-GBS internalization, hCMEC/D3 cells were pretreated with cytochalasin D (2 μM), nocodazole (1 μM), wortmannin (100 nM), MK2206 (2 μM), methyl-β-cyclodextrin (2.5 mM), or dynasore (80 μM) for 1 hour prior to infection with CC17-GBS. Inhibitors were left during the time of infection at the same concentration, except for dynasore, for which the concentration was dropped to 10 μM. Treatments did not affect bacterial or cell viability (data not shown).

Immunofluorescent staining and image analysis. hCMEC/D3 cells were grown on Thermanox coverslips (Thermo Fischer Scientific). Isolated brain microvessels were stuck to slides using Cell Tak (Corning). Infected or noninfected cells or isolated brain microvessels were fixed in PBS containing 4% paraformaldehyde (PFA) for 10 minutes. After fixation, samples were permeabilized by incubation in PBS containing 0.1% Triton X-100 for 4 minutes at room temperature, and then blocked for at least 1 hour at room temperature in PBS containing 10% serum. Primary antibodies diluted in 10% serum/PBS were incubated for at least 1 hour at room temperature. After 3 washes with PBS, samples were incubated for 1 hour at room temperature with conjugated secondary antibodies (Jackson ImmunoResearch Laboratories) diluted in PBS containing 10% serum. DAPI was used to counterstain nuclei, phalloidin-633 or -594 to stain actin, and isolectin B4–FITC to counterstain microvessels. After 3 washes in PBS, coverslips were mounted in DAKO fluorescent mounting media. Image acquisitions were realized using confocal laser scanning microscopy (Leica DMI6000) coupled to a spinning disk confocal head (Yokogawa CSU-X1M1), controlled by MetaMorph 7.7.5 software. Images were processed using ImageJ (NIH).

To distinguish between extracellular and intracellular bacteria, cells were infected with GFP-expressing bacteria. Extracellular GFP-expressing bacteria were counterstained in unpermeabilized conditions with an anti-GBS serum followed by a secondary rhodamine isothiocyanate–labeled antibody. Under these conditions, extracellular bacteria were green (GFP-labeled bacteria) and decorated with red (anti-GBS labeling), whereas intracellular bacteria were solely green (GFP-labeled bacteria).

Mechanical isolation of brain microvessels. Brain vessels from neonatal (2 days old), juvenile (3 weeks old), or adult (3 months old) rats or mice were isolated as described previously (69). Briefly, brains were collected and triturated in a Potter-Thomas homogenizer. The homogenate was centrifuged, and the pellet was resuspended in buffer containing 18% dextran. After centrifugation, myelin was eliminated and the pellet containing cerebral vessels was resuspended in a buffer containing 1% BSA. This suspension was filtered on a 20 μm nylon net filter and vessels fragments were recovered from the filter in a buffer containing 1% BSA. After final centrifugation, pellets of cerebral vessels were snap-frozen and kept at –80°C until used for Western blot analysis or fixed to glass slides for immunofluorescence using Cell Tak.

Collection of lateral and fourth ventricular choroid plexus. Choroid plexuses of lateral and fourth ventricles dissected from neonatal (2 days old) and adult rats under a stereomicroscope, as previously

described, were provided by the Brain Interface Exploratory Platform (BIP), Lyon Neuroscience Research Center (CNRL) (70). The collected tissues were snap-frozen and kept at –80°C until used.

Immunohistochemistry. Immunohistochemistry was performed by the HistIM facility (Histology, Immunostaining, laser, Microdissection) at the Cochin Institute. The paraffin-embedded brain sections were cleared before incubation in citrate buffer (pH 6.0). Expression of α5 or β3 integrin on sections was detected using the Bond Polymer Refine Detection kit (Leica Biosystems) with specific antibodies for α5 or β3 integrins and the immunostaining automaton (Bond III, Leica Biosystems). Pictures were acquired using the slide scanner (Lamina, PerkinElmer).

Animal experiments. Juvenile (3 weeks old) and adult (3 months old) BALB/c mice were infected by i.v. injection with 2×10^7 and 1.5×10^8 CFU, respectively, of exponentially growing GBS strains for 4 hours.

For some experiments, juvenile mice were pretreated by i.v. injecting either 10 μg of anti-α5 antibodies or isotype control, 5 mg/kg cyclic mimetic peptide RGDfV, or PBS 1 hour before challenge. No side effects in mice were observed after pretreatment targeting α5β1 or αvβ3 integrins. After 4 hours of infection, mice were euthanized, and blood, spleen, liver, and brain were collected. The brain and spleen were homogenized in 1 mL of 0.9% sodium chloride using a tissue homogenizer (Precellys system, Bertin Instruments) and the livers were homogenized in 9 mL using an Ultra-Turrax. Serial dilutions in 0.9% sodium chloride were immediately plated on TH agar for CFU counts. Bacterial counts in the mouse brains were corrected for blood contamination using the bacterial burden in the bloodstream and a conservative estimate of the mouse cerebral blood volume of 2.5 mL per gram of tissue as described previously (71).

To study the portal of entry into the brain of CC17-GBS, juvenile mice were perfused and brains were recovered and fixed overnight in PFA. The brains were embedded in 5% agarose and cut into 500 μm thick sections using a vibratome (Leica Biosystems). The brain sections were clarified using ethyl cinnamate (72) and immunostained using anti-CD31 (a marker for capillaries) and anti-transthyretin (TTR, a marker for choroid plexus) antibodies. The tissue sections were imaged using an Olympus IXplore Spin confocal microscope. Images were processed using ImageJ.

Statistics. All assays were performed in at least 3 independent experiments. Data represent mean ± SEM and statistical analyses were performed using GraphPad Prism 5.0. A P value less than 0.05 was considered significant.

Study approval. Written informed consent was obtained for all human samples used in this study. All animal experiments described in this study were conducted in accordance with the guidelines of Paris Descartes University, in compliance with the European animal welfare regulation (http://ec.europa.eu/environment/chemicals/lab_animals/home_en.html) and were approved by the Institut Cochin University Paris Descartes animal care and use committee (CEEA34; agreement 2018021616168438).

Author contributions

JG designed the research. RDDC, AP, ASB, CA, CC, AB, LC, and JG performed the experiments. GB performed in silico analysis of the BR_{Srr2}-α5β1 interaction. IP and CR provided anatomical pieces of human brain. ACB, MCS, and JG performed brain microvessel purification. JG, RDDC, AP, and AF analyzed the data. AF, AT, CP, EF, and CAR provided intellectual input and guidance. JG wrote the manuscript and AF, AT, and CP contributed to finalizing the manuscript. All authors discussed results and reviewed the final version of the manuscript.

Acknowledgments

We are grateful to Pierre-Olivier Couraud (INSERM, Paris, France) for the gift of hCMEC/D3 cells, Alain Duperray for the gift of CHO-ICAM1 cells, Yoshikazu Takada for the gift of CHO-αvβ3 cells, and Glen Ulett for the gift of the GFP plasmid. We are extremely grateful to Nathalie Strazielle and Jean-François Ghersi-Egea from BIP (CRNL, Lyon, France) for choroid plexus isolation and helpful comments. We thank Matthieu Benard from the animal facility of the Institut Cochin and Marine Gaillard for their help with animal experiments and Thomas Guilbert and Fabienne Regnier for their help with brain slice clarification. We also thank the Imag'IC and HistIM core facilities of the Cochin Institute and Shaynoor Dramsi for anti-Srr1 antibody and for critical reading of the manuscript. This work was supported by Agence Nationale de la Recherche (ANR; grant StrepB2brain, ANR-17-CE15-0026-01). LC is a recipient of a postdoctoral fellowship from the ANR (StrepB2brain). ASB is a doctoral fellow funded by Université de Paris. RDDC was funded by FERCM.

Address correspondence to: Julie Guignot, Institut Cochin, 22 rue Méchain 75014 Paris, France. Phone: 33.1.40.51.64.13; Email: julie.guignot@inserm.fr.

1. Da Cunha V, et al. 2014. Streptococcus agalactiae clones infecting humans were selected and fixed through the extensive use of tetracycline. *Nat Commun*. 2014;5:4544.
2. Russell NJ, et al. Maternal colonization with group B streptococcus and serotype distribution worldwide: systematic review and meta-analyses. *Clin Infect Dis*. 2017;65(suppl_2):S100–S111.
3. Edwards M, et al. Group B streptococcal infections. In: Remington J, et al. *Infectious Diseases of the Fetus and Newborn*. 7th ed. Expert Consult; 2010:419–469.
4. Joubrel C, et al. Group B streptococcus neonatal invasive infections, France 2007–2012. *Clin Microbiol Infect*. 2015;21(10):910–916.
5. Morinis J, et al. Horizontal transmission of group B streptococcus in a neonatal intensive care unit. *Paediatr Child Health*. 2011;16(6):e48–e50.
6. Hays C, et al. Perinatal hormones favor CC17 group B *Streptococcus* intestinal translocation through M cells and hypervirulence in neonates. *Elife*. 2019;8:e48772.
7. Tazi A, et al. Risk factors for infant colonization by hypervirulent CC17 Group B Streptococcus: toward the understanding of late-onset disease. *Clin Infect Dis*. 2019;69(10):1740–1748.
8. Lamy MC, et al. Rapid detection of the "highly virulent" group B Streptococcus ST-17 clone. *Microbes Infect*. 2006;8(7):1714–1722.
9. Manning SD, et al. Multilocus sequence types associated with neonatal group B streptococcal sepsis and meningitis in Canada. *J Clin Microbiol*. 2009;47(4):1143–1148.
10. Romain AS, et al. Clinical and laboratory features of group B streptococcus meningitis in infants and newborns: study of 848 cases in France, 2001-2014. *Clin Infect Dis*. 2018;66(6):857–864.
11. Seale AC, et al. Maternal colonization with streptococcus agalactiae and associated stillbirth and neonatal disease in coastal Kenya. *Nat Microbiol*. 2016;1(7):16067.
12. Coureuil M, et al. A journey into the brain: insight into how bacterial pathogens cross blood-brain barriers. *Nat Rev Microbiol*. 2017;15(3):149–159.
13. Kim BJ, et al. Bacterial induction of Snail1 contributes to blood-brain barrier disruption. *J Clin Invest*. 2015;125(6):2473–2483.
14. Nizet V, et al. Invasion of brain microvascular

endothelial cells by group B streptococci. *Infect Immun*. 1997;65(12):5074–5081.
15. Tazi A, et al. The surface protein HvgA mediates group B streptococcus hypervirulence and meningeal tropism in neonates. *J Exp Med*. 2010;207(11):2313–2322.
16. Six A, et al. Srr2, a multifaceted adhesin expressed by ST-17 hypervirulent group B streptococcus involved in binding to both fibrinogen and plasminogen. *Mol Microbiol*. 2015;97(6):1209–1222.
17. Seo HS, et al. Characterization of fibrinogen binding by glycoproteins Srr1 and Srr2 of Streptococcus agalactiae. *J Biol Chem*. 2013;288(50):35982–35996.
18. Seo HS, et al. Binding of glycoprotein Srr1 of streptococcus agalactiae to fibrinogen promotes attachment to brain endothelium and the development of meningitis. *PLoS Pathog*. 2012;8(10):e1002947.
19. Wang NY, et al. Group B streptococcal serine-rich repeat proteins promote interaction with fibrinogen and vaginal colonization. *J Infect Dis*. 2014;210(6):982–991.
20. Bang JY, et al. Pharmacoproteomic analysis of a novel cell-permeable peptide inhibitor of tumor-induced angiogenesis. *Mol Cell Proteomics*. 2011;10(8):M110 005264.
21. Ruoslahti E. RGD and other recognition sequences for integrins. *Annu Rev Cell Dev Biol*. 1996;12:697–715.
22. Choi Y, et al. Site-specific inhibition of integrin alpha v beta 3-vitronectin association by a ser-asp-val sequence through an Arg-Gly-Asp-binding site of the integrin. *Proteomics*. 2010;10(1):72–80.
23. Hynes RO, et al. The diverse roles of integrins and their ligands in angiogenesis. *Cold Spring Harb Symp Quant Biol*. 2002;67:143–153.
24. Paulus W, et al. Characterization of integrin receptors in normal and neoplastic human brain. *Am J Pathol*. 1993;143(1):154–163.
25. Wang J, Milner R. Fibronectin promotes brain capillary endothelial cell survival and proliferation through α5β1 and αvβ3 integrins via MAP kinase signalling. *J Neurochem*. 2006;96(1):148–159.
26. Zhang K, Chen J. The regulation of integrin function by divalent cations. *Cell Adh Migr*. 2012;6(1):20–29.
27. Bolduc GR, Madoff LC. The group B streptococcal alpha C protein binds α1β1-integrin through a novel KTD motif that promotes internalization of GBS within human epithelial cells. *Microbiology (Reading)*. 2007;153(pt 12):4039–4049.
28. Zeng H, et al. ComplexContact: a web server for inter-protein contact prediction using deep learning. *Nucleic Acids Res*. 2018;46(W1):W432–W437.
29. Schreiner CL, et al. Isolation and characterization of Chinese hamster ovary cell variants deficient in the expression of fibronectin receptor. *J Cell Biol*. 1989;109(6):3157–3167.
30. Guignot J, et al. Human decay-accelerating factor and CEACAM receptor-mediated internalization and intracellular lifestyle of Afa/Dr diffusely adhering Escherichia coli in epithelial cells. *Infect Immun*. 2009;77(1):517–531.
31. Takagi J, et al. Changing ligand specificities of alphavbeta1 and alphavbeta3 integrins by swapping a short diverse sequence of the beta subunit. *J Biol Chem*. 1997;272(32):19794–19800.
32. Sans E, et al. Analysis of the roles of ICAM-1 in neutrophil transmigration using a reconstituted mammalian cell expression model: implication of ICAM-1 cytoplasmic domain and Rho-dependent signaling pathway. *J Immunol*. 2001;166(1):544–551.
33. Bhattacharya S, et al. α(v)β(3) integrin induces tyrosine phosphorylation-dependent Ca(2+) influx in pulmonary endothelial cells. *Circ Res*. 2000;86(4):456–462.
34. Conforti G, et al. Human endothelial cells express integrin receptors on the luminal aspect of their membrane. *Blood*. 1992;80(2):437–446.
35. Singh B, et al. Vascular expression of the α(v) β(3)-integrin in lung and other organs. *Am J Physiol Lung Cell Mol Physiol*. 2000;278(1):L217–L226.
36. Xanthis I, et al. β1 integrin is a sensor of blood flow direction. *J Cell Sci*. 2019;132(11):jcs229542.
37. van Kassel MN, et al. Community-acquired group B streptococcal meningitis in adults: 33 cases from prospective cohort studies. *J Infect*. 2019;78(1):54–57.
38. Luan SL, et al. Multilocus sequence typing of Swedish invasive group B streptococcus isolates indicates a neonatally associated genetic lineage and capsule switching. *J Clin Microbiol*. 2005;43(8):3727–3733.
39. Strazielle N, Ghersi-Egea JF. Choroid plexus in the central nervous system: biology and physiopathology. *J Neuropathol Exp Neurol*. 2000;59(7):561–574.
40. Yang JT, et al. Embryonic mesodermal defects in alpha 5 integrin-deficient mice. *Development*. 1993;119(4):1093–1105.
41. Iovino F, et al. pIgR and PECAM-1 bind to pneumococcal adhesins RrgA and PspC mediating bacterial brain invasion. *J Exp Med*. 2017;214(6):1619–1630.
42. Su G, et al. Absence of integrin αvβ3 enhances vascular leak in mice by inhibiting endothelial cortical actin formation. *Am J Respir Crit Care Med*. 2012;185(1):58–66.
43. Tibussek D, et al. Late-onset group B streptococcal meningitis has cerebrovascular complications. *J Pediatr*. 2015;166(5):1187–1192.
44. Kohli-Lynch M, et al. Neurodevelopmental impairment in children after group B streptococcal disease worldwide: systematic review and meta-analyses. *Clin Infect Dis*. 2017;65(suppl_2):S190–S199.
45. Andrade EB, et al. A mouse model reproducing the pathophysiology of neonatal group B streptococcal infection. *Nat Commun*. 2018;9(1):3138.
46. Wang X, et al. Integrin alphavbeta3 is a coreceptor for human cytomegalovirus. *Nat Med*. 2005;11(5):515–521.
47. Humtsoe JO, et al. A streptococcal collagen-like protein interacts with the alpha2beta1 integrin and induces intracellular signaling. *J Biol Chem*. 2005;280(14):13848–13857.
48. Weckel A, et al. The N-terminal domain of the R28 protein promotes *emm28* group A Streptococcus adhesion to host cells via direct binding to three integrins. *J Biol Chem*. 2018;293(41):16006–16018.
49. Gianni T, et al. αVβ3-integrin routes herpes simplex virus to an entry pathway dependent on cholesterol-rich lipid rafts and dynamin2. *Proc Natl Acad Sci U S A*. 2010;107(51):22260–22265.
50. Kumar D, et al. Intravital imaging of vascular transmigration by the lyme spirochete: requirement for the integrin binding residues of the B. burgdorferi P66 protein. *PLoS Pathog*. 2015;11(12):e1005333.
51. Ristow LC, et al. Integrin binding by Borrelia burgdorferi P66 facilitates dissemination but is not required for infectivity. *Cell Microbiol*. 2015;17(7):1021–1036.
52. Alghisi GC, et al. The integrin antagonist cilengitide activates αVβ3, disrupts VE-cadherin localization at cell junctions and enhances permeability in endothelial cells. *PLoS One*. 2009;4(2):e4449.
53. Engelhardt B. β1-integrin/matrix interactions support blood-brain barrier integrity. *J Cereb Blood Flow Metab*. 2011;31(10):1969–1971.
54. Hermann DM, ElAli A. The abluminal endothelial membrane in neurovascular remodeling in health and disease. *Sci Signal*. 2012;5(236):re4.
55. Osada T, et al. Interendothelial claudin-5 expression depends on cerebral endothelial cell-matrix adhesion by β(1)-integrins. *J Cereb Blood Flow Metab*. 2011;31(10):1972–1985.
56. Pulous FE, Petrich BG. Integrin-dependent regulation of the endothelial barrier. *Tissue Barriers*. 2019;7(4):1685844.
57. Kim BJ, et al. Modeling group B streptococcus and blood-brain barrier interaction by using induced pluripotent stem cell-derived brain endothelial cells. *mSphere*. 2017;2(6):e00398–17.
58. Davalos D, Akassoglou K. Fibrinogen as a key regulator of inflammation in disease. *Semin Immunopathol*. 2012;34(1):43–62.
59. Hauck CR, et al. Exploitation of integrin function by pathogenic microbes. *Curr Opin Cell Biol*. 2012;24(5):637–644.
60. Banerjee A, et al. Bacterial Pili exploit integrin machinery to promote immune activation and efficient blood-brain barrier penetration. *Nat Commun*. 2011;2:462.
61. Dramsi S, et al. Epidemiologically and clinically relevant group B streptococcus isolates do not bind collagen but display enhanced binding to human fibrinogen. *Microbes Infect*. 2012;14(12):1044–1048.
62. Vornhagen J, et al. Group B streptococcus exploits vaginal epithelial exfoliation for ascending infection. *J Clin Invest*. 2018;128(5):1985–1999.
63. Brochet M, et al. Genomic diversity and evolution within the species streptococcus agalactiae. *Microbes Infect*. 2006;8(5):1227–1243.
64. Phares CR, et al. Epidemiology of invasive group B streptococcal disease in the United States, 1999–2005. *JAMA*. 2008;299(17):2056–2065.
65. Kalimuddin S, et al. 2015 epidemic of severe streptococcus agalactiae sequence type 283 infections in Singapore associated with the consumption of raw freshwater fish: a detailed analysis of clinical, epidemiological, and bacterial sequencing data. *Clin Infect Dis*. 2017;64(suppl_2):S145–S152.
66. Milner R, Campbell IL. Developmental regulation of β1 integrins during angiogenesis in the central nervous system. *Mol Cell Neurosci*.

2002;20(4):616–626.
67. Raab-Westphal S, et al. Integrins as therapeutic targets: successes and cancers. *Cancers (Basel)*. 2017;9(9):110.
68. Weksler B, The hCMEC/D3 cell line as a model of the human blood brain barrier. *Fluids Barriers CNS*. 2013;10(1):16.
69. Boulay AC, et al. Purification of mouse brain vessels. *J Vis Exp*. 2015;(105):e53208.
70. Kratzer I, et al. Developmental changes in the transcriptome of the rat choroid plexus in relation to neuroprotection. *Fluids Barriers CNS*. 2013;10(1):25.
71. Doran KS, et al. Group B streptococcal beta-hemolysin/cytolysin activates neutrophil signaling pathways in brain endothelium and contributes to development of meningitis. *J Clin Invest*. 2003;112(5):736–744.
72. Vigouroux R, et al. Neuroscience in the third dimension: shedding new light on the brain with tissue clearing. *Mol Brain*. 2017;10(1):33.